NASA

Technical Memorandum 83837

# A Large Scale Height Galactic Component of the Diffuse 2-60 keV Background

D. Iwan, F. E. Marshall, E. A. Boldt,
R. F. Mushotzky, R. A. Shafer,
and A. Stottlemyer



MARCH 1982

National Aeronautics and
Space Administration

**Goddard Space Flight Center**
Greenbelt, Maryland 20771

# A LARGE SCALE HEIGHT GALACTIC COMPONENT OF THE DIFFUSE 2-60 keV BACKGROUND

DeAnn Iwan[1], F.E. Marshall, E.A. Boldt, R.F. Mushotzky,
R.A. Shafer[1], and A. Stottlemyer[2]

Laboratory for High Energy Astrophysics
NASA/Goddard Space Flight Center
Greenbelt, Maryland 20771

## ABSTRACT

The diffuse 2-60 keV X-ray background has a galactic component clearly detectable by its strong variation with both galactic latitude and longitude. This galactic component is typically 10% of the extragalactic background towards the galactic center, half that strong towards the anticenter and extrapolated to a few percent of the extragalactic background towards the galactic poles. It is acceptably modeled by a finite radius emission disk with a scale height of several kiloparsecs. The averaged galactic spectrum is best fit by a thermal spectrum of kT ≈ 9 keV, a spectrum much softer than the ≈ 40 keV spectrum of the extragalactic component. The most likely source of this emission is low luminosity stars with large scale heights such as subdwarfs. Inverse Compton emission from GeV electrons on the microwave background contributes only a fraction of the galactic component unless the local cosmic ray electron spectrum and intensity are atypical.

Subject headings: galaxies: stellar content - stars: subdwarfs -.
X-rays: sources

[1]Also Dept. of Physics & Astronomy, Univ. of Maryland

[2]Computer Science Corporation

# I. INTRODUCTION

The largest feature of the diffuse 2-60 keV X-ray background is due to our Galaxy. This galactic component contributes from ≈ 2% to 10% of the total X-ray background intensity. It is easily separated from the extragalactic component by its strong spatial dependence on galactic longitude and latitude and by its distinctly softer spectrum.

The total diffuse X-ray background between 2 and 60 keV is largely isotropic. For example, Schwartz et al. (1976) reported the sky to be isotropic with intrinsic fluctuations of only ≈ 3% over an effective solid angle of 0.004 steradians at 2-10 keV when known discrete sources were eliminated and when areas within $20^{0}$ of the galactic plane were excluded. Indications of a galactic component contributing to the count-rates at low latitudes have been found in both the Uhuru data (e.g. Schwartz et al. 1976; Protheroe, Wolfendale and Wdowczyk 1980) and Ariel V data (Warwick et al. 1980). In the HEAO 1 A-2 data base this galactic component is clearly seen to have a longitude dependence as well as a latitude dependence.

The spatial variations of the dominant galactic component are satisfactorily described by a finite radius disk of X-ray emission with an X-ray scale height of several kiloparsecs. Any other large scale spatial features are smaller than about 3% of the total intensity.

A composite spectrum of the Galaxy can be obtained by taking the spectrum obtained at low latitudes and subtracting out the spectrum seen at high latitudes. The best fit is obtained for an optically thin thermal bremsstrahlung spectrum of ≈ 9 keV (≈ 100 million Kelvins). This averaged spectrum is much softer than the ≈ 40 keV spectrum seen at high latitudes (Marshall et al. 1980).

## II. THE EXPERIMENT

The A-2 instrument on the HEAO 1 spacecraft provides far more detailed spatial and spectral information on the diffuse background than do previous instruments for several reasons. 1) The detectors have a lower internal background than previous instruments. The HED1 and HED3 detectors have a particle veto layer which reduces the instrument's response to electrons by two orders of magnitude. In addition, all detectors provide a variety of data selection criteria to further reduce contamination. 2) The entire sky was scanned 2 2/3 times, once every 6 months, with roughly uniform coverage. These separate scans of the sky have been tested for consistency. 3) The instrument contains an ensemble of 4 detectors of different fields of view (fov) and of different energy bandpasses. These separate detectors have also been used for consistency checks. 4) Each detector has 2 fields of view, over alternate anode wires. HED1 has both a $3^0 \times 6^0$ and a $3^0 \times 3^0$ fov while the MED and HED3 have $3^0 \times 3^0$ and $3^0 \times 1\ 1/2^0$ fov. By subtracting the small fov data from the large fov data, the internal background can, on a moment by moment basis, be essentially eliminated.

More detailed descriptions of the A2 instrument are given in Rothschild et al. (1979) and Marshall et al. (1980). Data reported here come from three of the six proportional counters, HED1, MED and HED3. The two HED counters are $\sim 800$ cm$^2$ xenon counters with a propane anticoincidence layer contained between two 1 mil. mylar windows. These counters have a response from 2-60 keV. The MED is a $\sim 800$ cm$^2$ argon counter with a response from 2-20 keV. The principal counter used in this analysis is the HED1 because it has a larger fov and hence better counting statistics. The results from MED and HED3 are consistent with the results from HED1.

## III. DATA SELECTION

Data are excluded whenever a known source is in the field of view (as determined by the HEAO 1 A2 catalogue of detected sources which is complete to better than $\approx 5 \times 10^{-11}$ erg/(cm$^2$-s) in the 2-10 keV band). The analysis presented here is for large-minus-small fov; this eliminates most of the internal background. Other criteria for "clean" data, such as eliminating time frames with high electron contamination potential (as determined by high veto rates), are also used. This source-free data base is termed "diffuse" throughout this paper, without making reference to the actual nature of the emission regions involved.

Spatial analysis is done on data obtained in the mission from day 322 to day 697 of 1977. This results in an exposure of $\approx$ 2 million cm$^2$-s-sr for the HED1 large-minus-small fov. As an additional check, analysis is done separately on two scans of the sky. Both of these scans are consistent for each of the counters in that the intensities of the source-free regions of any scan of the sky could be satisfactorily predicted from another scan as

1) Intensity ($\ell$,b,scan i,detector k) = F x
Intensity ($\ell$,b,scan j, detector $\ell$) + A

where "F" is a constant of value $\approx$ 1.0, where "A" is set to 0 when a single detector is used and where "$\ell$", "b" are galactic coordinates. F differs slightly from 1 because there is a slow drift in counter efficiency with time and a small discontinuity in efficiency around day 544 when the low energy detectors were turned off. These efficiency drifts are on the order of 1% per 6 months. The offset parameter A is introduced when different counters are compared to take into account the different energy responses of the individual detectors. Table 1 shows some specific examples of these comparisons.

Note that the excellent agreement between maps produced 6 months apart

implies that no long term (6 month) temporal fluctuations are seen in the source free sky when taken as a whole. In other words, the intensity of a typical pixel in one scan of the sky for HED1 is within the average sigma (≈ 3.5 %) from Poisson counting statistics of that same $3^0$ x $3^0$ pixel when observed 6 months later. Were temporal fluctuations typically a sizable fraction of the poisson errors, successive scans of the sky would not have been so consistent.

The spectral data presented here are for the first scan of the sky only (days 322-542 of 1977) in order to keep the efficiency discontinuity around day 544 from distorting the spectra.

## IV. SPATIAL ANALYSIS OF THE DATA

The first step in the spatial analysis is to map the X-ray data onto an Aitoff projection in galactic coordinates in $3^0$ x $3^0$ pixels. Whenever a counter's center of fov is in a given pixel, that pixel receives the data. A map is constructed for the entire energy bandpass of each counter and for each of three separate energy bands of HED 1 as described below. These maps are then used as the data base for all spatial analysis. The most detailed analysis is done on the entire bandpass of the HED 1 counter because of its superior statistics. The conclusions derived are also consistent with those for each individual energy band of HED 1 and for each of the other counters when the spectrum of the galactic component is taken into account.

Figure 1 is the HED 1 map of the sky, but binned on a coarser ($9^0$ x $9^0$) scale so that the large scale features may be more readily seen and so that the map can be more readily compared with the Uhuru and Ariel V maps. Coverage varies over the map, but the median standard deviation on this scale is ≈ 1.5% of the mean intensity (i.e., one line per pixel). Pixels with standard deviations greater than 3 3/4% (2 1/2 lines per pixel) are separated

off with dashed lines.

The X-ray intensity shows a strong dependence on galactic coordinates. Figure 2a shows the count-rate for the entire HED1 counter bandpass (2-60 keV) as a function of galactic latitude. Data are divided into two longitude bins, the diamonds representing data from $\ell = -90^0$ to $\ell = +90^0$ (towards galactic center) and the crosses representing data taken from $\ell = 90^0$ to $\ell = 270^0$ (towards the anticenter). It is this galactic component we discuss here. Other features, such as the slightly higher fluxes in the Northern than Southern hemisphere will be discussed in subsequent papers. (These other features are smaller than ~ 2% of the total background. They are referred to in this paper as "second order effects").

Figures 2b through 2d show the count-rate for three energy bands within the HED1 detector. The highest energy band comes from taking only the second layer of the counter (Figure 2d). This layer has a response primarily from 6-60 keV, peaking around 13 keV. Layer 1 is divided into two energy bands by a discriminator set at ~ 7.5 keV, just above the iron line (at 6.7 keV). The softest band (labeled AB in Figure 2b) has a response primarily from 2-10 keV, peaking around 5 keV. The intermediate band (labeled CD in Figure 2c) has a spectral response primarily from 5-20 keV, peaking around 8 keV. Note, however, that while these bands provide crude energy separation, they are all overlapping. Detailed spectral analysis can better be done from the pulse height data. Crude spectral analysis from these three bandpasses agrees with the pulse height analysis presented here.

Figure 3e is a plot of intensity versus the absolute value of the galactic longitude ( i.e., $\ell = -30^0 \equiv \ell = +30^0$) for various absolute latitude bins. That is, the four "quadrants" of the Galaxy are folded together so that the average effects due to the Galaxy are more readily

apparent. The latitude bin from $0^0$ to $6^0$ is strongly affected by source removal and should be viewed with extreme caution. Notice that even at high latitudes there is still a longitude dependence to the intensities.

The data shown in Figure 3e imply that a disk model for the Galaxy is more appropriate than a spheroidal halo model because the intensity increases towards the plane for all longitudes. Further, an infinite uniform disk model is inappropriate because such a disk would give no longitude dependence, whereas Figure 4 quite clearly shows longitudinal variation.

A simple model of the Galaxy which could produce the longitude and latitude dependence seen is that of a finite radius disk of emission. In this model, X-ray emission interior to the disk radius depends only on scale height (i.e., the emission has an exponential dependence on z, the distance above the plane) and there is no galactic X-ray emission exterior to the disk radius. The total X-ray intensity (galactic and extragalactic) is given by:

$$2) \quad I_{total}(\ell, b) = I_o + \frac{Eh}{R_{gc}\sin|b|}\{1-\exp[-x.\tan|b|.R_{gc}/h)\} \text{ counts s}^{-1}$$

$$\text{in which } x = \cos\ell + [(R_d/R_{gc})^2 - \sin^2\ell]^{1/2}$$

where $I_0$ is the average isotropic extragalactic count-rate assumed by this model, $\ell$ is galactic longitude, b is galactic latitude, h is the scale height of the X-ray emission, $R_{gc}$ is the distance to galactic center (taken to be 10 kpc), E is the normalization constant for the galactic emission relative to the extragalactic emission, and $R_d$ is the radius of the emission disk.

The total intensity, $I_{total}$, is plotted in Figure 3 for several combinations of h and R on the same scale as the observations in Panel 3e. Note that away from the plane ($|b| \gtrsim 10^0$) the variation with longitude is only

apparent when data with $|\ell| < 90^{o}$ are included and that little variation is apparent at high latitudes ($|b| \gtrsim 30^{o}$).

Determinations of the goodness-of-fit of any model for the diffuse X-ray sky are complicated by the variance introduced by the intrinsic fluctuations in the sky. Schwartz (1979) estimates these fluctuations as ~ 3% of the background intensity 2-10 keV in the bandpass for an effective solid angle of 4 msr. A correct method of including the effect of these intrinsic fluctuations (particularly if the nongaussian nature of the distribution is to be considered) is an involved task and depends on the model used for the source distribution of the fluctuations. Instead, for purposes of estimating the goodness-to-fit of the models discussed here, we use the sky above $45^{o}$ latitude to estimate the "noise" which the intrinsic fluctuations introduce into the maps. This noise term is then added in quadrature to the Poisson counting statistics errors of each pixel. That is, the total variance over the map, $T^2$, is a sum of three parts:

$$3) \quad T^2 = F^2 + P^2 + I^2$$

where $F^2$ is the variance of the intrinsic sky fluctuations, $P^2$ is the variance of the counting statistics alone and $I^2$ is the variance introduced by systematic effects such as residual internal background. For the large-minus-small fov data considered here, $I^2$ is much smaller than the other variances and may be considered to be zero.

From the high latitude data, we estimate that the intrinsic fluctuations on the sky introduce a noise of ~ 1.84% between the pixels. This compares to ~ 3.5% for the typical error introduced by counting statistics. When the remainder of the sky (that is, latitudes below $45^{o}$) is fit to a finite disk

model, this noise term is added in. Neither the exact value of $F^2$ used nor the exact latitude range selected for the fits to the disk model significantly affects the acceptable range of disk parameters. That is, fits from $10^0$ to $45^0$, $0^0$ to $45^0$ and $0^0$ to $90^0$ all imply about the same range of parameters.

The best fit model to the sky from $0^0$ to $45^0$ latitude is found to be $I_b$ = 5.12c/s, E = 3.14% of $I_b$, h = 0.73 $R_{gc}$, $R_d$ = 2.8$R_{gc}$, giving a chi-squared of 3241.46 for 3026 degrees of freedom. Since the expected distribution of chi-squared for so many degrees of freedom is roughly Gaussian, 1 sigma in chi-squared is ≈ 55. Thus the above fit is marginally acceptable (at ≈ 3.9 sigma). When the largest 'second order' feature is considered, chi-squared drops by several hundred, implying a much better fit to the data. Second order features will be discussed in subsequent papers. While such second order effects can change the details of the galactic model's fit, these other features do <u>not</u> change the gross aspects of the fits presented here.

Figure 5 shows the formal 95% confidence contours for the scale height and disk radius parameters (as determined by taking the minimum chi-squared plus 5.99) Preliminary analysis of the large-plus-small fov data indicates that the lower portion of this range (h ≈ 3 kpc) is probably the more applicable portion. The true 95% confidence contours for the finite disk model would be larger since we have neglected the effects of the "second order" features.

Figure 3 gives the chi-squared values for several choices of parameters for the model. Table 2 gives a summary of parameters of interest for acceptable disk parameters implied by the data. Note that the large range of implied galactic luminosities is due to the large variation in the implied emission volume. The emissivity in the plane and the flux towards zenith are not strong functions of the disk parameters.

The estimated intensities for the galactic emission from other observers are within the range of acceptable (3 sigma) fits to our data. These estimates are, however, lower than our best fit model. Warwick et al. 1980, fit the Ariel V data to an infinite disk (they saw no evidence for longitudinal dependence) with a local surface emissivity towards the poles of 2.5% of their diffuse background, ($\approx 1.5 \times 10^{-8}$ erg-s$^{-1}$-cm$^{-2}$ at 2-10 keV). This compares with our best fit value of $2.3 \times 10^{-8}$ erg-s$^{-1}$-cm$^{-2}$ (also at 2-10 keV). Warwick et al. set an upper limit of "$\lesssim$ 1 Kpc" for the scale height of a thick disk with an assumed radius of 15 Kpc. As can be seen in Figure 5 the best fit scale height strongly depends on the assumed disk radius. Although larger radii are preferred, an assumed radius of 15 Kpc would lead to a best fit scale height of about 1.4 Kpc using the HEAO A2 observations. Although this value apparently contradicts the value of Warwick et al., it should be remembered that 1) Warwick et al. did not include data within $20^{0}$ of the galactic plane where the longitudinal variation is the largest, 2) "second order" effects were not included in either analyses, and 3) the precise determination of statistical uncertainties is difficult because of the need to approximate the effect of fluctuations. Protheroe et al. (1980) fit a different disk model to data from the Uhuru satellite. An exponential radial dependence was fit to the emissivity as well as the usual exponential scale height. Disk emission was truncated at 15 Kpc. The best fit exponential scale height was $1.6^{+3}_{-1.3}$ Kpc which would appear to be consistent with the results reported herein. The local surface emissivity was $0.8 \times 10^{-9}$ erg s$^{-1}$ cm$^{-2}$ (2 to 7 keV) or about half that seen with HEAO A2. This difference is probably due at least in part to the assumed radial dependence of the model of Protheroe et al. in which emissivity is substantially larger near the galactic center.

Note that the galactic component we see extends to high latitudes and is distinct from the narrower disk component seen by Bleach et al. (1972) and Wheaton (1976). The disk seen by Bleach et al. is only a few degrees in extent, while the model parameters presented here are determined primarily by the data between $10^0$ and $40^0$ latitude. The narrow disk component of Bleach et al. is also much stronger, about 30% of the isotropic intensity. The "thin disk" component has also been seen in the HEAO 1 A2 data base when finer angular resolution is used (Worrall et al. (1982)). The model in Figure 3a is for "thin disk" parameters like that suggested by the very narrow band of emission seen in the galactic plane by Bleach et al. (1972) and Worrall et al. (1982). This figure shows that such a low scale height (< 500 pc) model does not fit the high latitude data. While the thin disk component probably has a scale height less than about 500 pc, the thick disk discussed in this paper probably has a scale height greater than about 1500 pc. (Figure 5 indicates a scale height > 2000 pc at the 95% confidence limits. However, other large scale features on the sky may change this limit somewhat.)

When a composite disk possessing two scale heights is used, the parameters of the larger scale height component are not changed much by the addition of a "thin" disk component. The intensity of the thicker disk drops by 20% or 30% and the disk radius decreases. Other features can also interfere with the two component disk model. Modeled enhancemen for the supercluster, galactic center region, North Polar Spur, Compton-Getting effect for the cosmic background, composite scale heights and the like all compete with each other. Subsequent papers will discuss these components. Still, the dominant anisotropic component is always approximately that of the single scale height finite radius disk model we present here.

Figure 3f shows the composite disk model for scale heights of both 450 pc

and 3 kpc. Parameters of interest for this model are included in Table 2. Note that the emission in the larger scale height component has decreased by only 20% from the single scale height fit.

Because of interference from other features, it is difficult to place limits on the range and intensity of the possible components of such a composite disk. As a rule of thumb, if the scale height of both components is fixed at an optimum combination, the intensity of either component may be varied by a factor of 2 and the other will be able to compensate satisfactorily. Similarly, if one of the scale heights is fixed, the other may be varied by a factor of about 2.

Because of the uncertainties and complexities involved in detailing a two component disk, we will continue to discuss the data in terms of a single (large) scale height disk, keeping in mind that we may be overestimating the strength of this component.

Other models of the Galaxy which were tried failed to produce an acceptable fit to the data for reasonable values of their parameters. An isotropic, spherical halo, for example, yielded chi-squareds twice those of the disk models. Using a Schmidt model for the mass ellipsoids of the Galaxy and assuming an X-ray luminosity proportional to mass also gave a very poor fit with chi-squareds hundreds higher as did models where the disk had a radial exponential scale height as well as a vertical scale height. A composite model of finite disks of normal dwarf stars (with independent optical to X-ray luminosity ratios for each scale height range of the stars) fit poorly for any reasonable range of disk radii.

The problem of modeling the smaller features to obtain either a better galactic model or estimates of cosmic parameters such as the Compton-Getting effect can be readily seen by examining Figure 6. This figure shows the

longitude dependence of the count-rates within $30^0$ of the Galactic plane, where we expect the Galaxy to dominate the spatial distribution of the flux. Note, for example, that the lowest count-rates are seen, not at the galactic anticenter, but near $120^0$ longitude. (This variation is not an artifact of source removal; it occurs at all latitudes). To examine effects smaller than ~ 3% of the isotropic background, we must go to a larger data base than that used here.

## V. SPECTRAL ANALYSIS

The averaged spectrum of the galactic component is obtained by taking the spectrum at low latitudes ($-20^0 < b < 20^0$) and subtracting the background (presumed isotropic) spectrum seen above $45^0$ latitude (where the galactic contribution is small). This background spectrum is approximately the 40 keV spectrum determined for latitudes above $20^0$ by Marshall et al. 1980. To combine spectra taken over a wide range of latitudes, a correction is made for the average galactic absorption ($3 \times 10^{20}$ atoms/cm$^2$ x csc $|b|$). This averaged low latitude, galactic spectrum is thus the sum of many components (e.g., bulge sources, thick disk sources, thin disk sources).

A simple single temperature thermal model provides a good fit to the high latitude data, but not to the low latitude data ($\chi^2$ of 316 for 22 degrees of freedom). Adding a single simple power law spectrum to the low latitude model helps, but the fit is still bad ($\chi^2$ of 82 for 19 degrees of freedom if additional absorption is allowed, $\chi^2$ of 151 for 20 dof if no additional absorption is allowed). However, if a second temperature component is tried instead of a power law component, a very good fit is obtained ($\chi^2$ = 20.02 for 20 dof). The best fit thermal spectrum is 9 keV ± 1.5 keV (95% confidence) with no absorption in addition to the average galactic absorption described above. A 1.2% systematic uncertainty in the counter response function is

included in these fits.

Clearly a thermal model is the preferred simple model for the averaged galactic spectrum. Once such a thermal model is included, a power law component can be added in without making the fits unacceptable. Figure 8 shows the 95% confidence upper limits to the percentage of the averaged galactic spectrum which can be a power law for various spectral indices. Both temperatures, 9 keV and 40 keV, have been fixed. If the temperatures are allowed to vary substantially, larger power law components can be introduced into the fits.

A double power law spectrum of the form

$$4) \quad \text{Flux} \propto E^{-a_1} e^{-N_H\sigma} \qquad E < E_{cutoff}$$

$$\propto E^{-\alpha_2} e^{-N_H\sigma} \qquad E > E_{cutoff}$$

was also tried. Such a double power law model could fit the data well only if the second power law was allowed to be very steep ($\alpha_2 > 2.7$). The best fit obtained was for $\alpha_1 = 1.85$, $\alpha_2 = 2.82$, $E_{cutoff} = 11$ keV yielding a $\chi^2$ of 16.17.

If the spectral indices were constrained to lie within the range implied by the cosmic ray electron spectrum seen at the Earth for the inverse Compton emission mechanism (that is, $1.57 < \alpha_1, \alpha_1 < \alpha_2, \alpha_2 < 2.2$ for electron indices between 2.14 and 3.4), then the fit was poor. The best fit in this case was $\alpha_1 = 2.0$, $\alpha_2 = 2.2$, $E_c = 5$ keV yielding a $\chi^2$ of 164.

When such a component is added to a thermal component for the galactic emission, the thermal component dominates the emission. The temperature converges to 8 1/2 keV and the double power law to effectively that of a

single power law of index 2.2. Thus the upper limits of Figure 8 apply to this double power law model, too.

No iron line is seen at 6.7 keV. The 95% upper limit is 150 eV equivalent width. An equivalent width of 900 eV would be expected for solar abundances if a single optically thin thermal emission process comprised the entire averaged galactic spectrum.

## VI. INTERPRETATIONS

The X-ray luminosity of the Galaxy implied by the finite radius disk model is about 8 x $10^{38}$ ergs/s from 2-20 keV (to within a factor of ~ 3). This luminosity is comparable to the upper limit luminosity of ~ $10^{39}$ ergs/s from nearby normal type galaxies (Worrall et al. 1979) and to the summed emissivity of known sources for our own Galaxy of ~ 2 x $10^{39}$ ergs/s (Worrall et al. 1979). Clearly this "diffuse" component is not negligible.

Three main types of models hold promise of supplying this X-ray emissivity. 1) The X-ray emission could be due to point sources in the Galaxy which have large scale heights (> 1500 pc), 2) The X-ray emission could come from a halo of very hot (~ $10^8$ $^oK$) gas, 3) The X-ray emission could come from inverse Compton emission from cosmic ray electrons off of the microwave background. These three models will be discussed in detail below.

Any other model proposed must fit available data in the hard X-ray and at other wavelengths (notably, radio, gamma-ray, and soft X-ray). In particular, models which would give a very small scale height to the hard X-ray emission (such as the bremsstrahlung of cosmic rays off of cool gas, as Stecker (1977) and others have proposed for the gamma-ray emission) are regarded here as very unlikely to provide the large scale height X-ray emission observed. The spatial fitting of the X-ray data is taken to eliminate models whose scale heights are determined by cool gas, main sequence dwarf stars, white dwarfs

and any other models with scale heights < 500 pc. It is, of course, always conceivable that some very local phenomenon is somehow simulating a finite radius disk of hard X-ray emission which only looks like it must be of galactic scale. We do not, however, consider this possibility further.

In the following discussion we make the tacit assumption that the emission that dominates the spatial feature of the galactic emission also dominates the averaged spectral feature. This assumption may not be valid, because 1) the averaged spectrum is a combination of that of the thick disk with that of other components and 2) the spectra of these different components may be quite different. Rather than continually reiterate these caveats, we will assume the simple case and proceed with our discussion as if this useful assumption were true.

## VII. POINT SOURCE MODELS

The X-ray disk emission may be produced by low luminosity point sources. However, most known galactic point sources of hard X-rays are associated with Population I objects and so are confined to the galactic plane. For example, normal dwarf (luminosity class V) stars have scale heights less than 400 pc. White dwarfs have scale heights of ~ 500 pc. Stars with scale heights of a few hundred parsecs doubtless contribute to the thin disk seen by Bleach et al. (1972) and Worrall et al. (1982) but those scale heights are inconsistent with the thick finite radius disk models discussed here.

Most point sources with large scale heights have space densities too small to provide the modeled X-ray intensity of (3-6) x $10^{25}$ ergs $s^{-1}$ $pc^{-3}$. For example, globular clusters have a scale height of ~ 3000 pc, but are spherically symmetric and have space densities less than $10^{-6}$ $M_{\odot}$ $pc^{-3}$. Most other Population II objects, like RR Lyrae stars, have similar low space

densities. Only subdwarfs (luminosity class VI) have high enough scale height (~ 2000 pc) and high enough space density to be good candidates for the observed emission. These halo stars, extreme Population II objects, are subluminous in the optical bandpass, have low metallicities, and have high space velocities.

At present any estimates of the X-ray volume emissivity of subdwarfs is necessarily uncertain since neither the space density or average luminosity of subdwarfs is known. The space density typically given for subdwarfs is ~ 1.6 x $10^{-3}$ $M_0$ $pc^{-3}$ (e.g. Allen 1973), but this is not a well-determined quantity. This space density would require a 2-20 keV X-ray luminosity of 1.9 to 3.8 x $10^{28}$ ergs $s^{-1}$ $M_0^{-1}$ but very little is known about their average X-ray luminosity. Johnson's (1981) study of stars within 6.3 pc of the sun using the Einstein Observatory's imaging instruments includes 3 stars classified as subdwarfs. One of these is detected at 1.4 x $10^{27}$ ergs $s^{-1}$ in the 0.2-4.0 keV Einstein energy band while the others have similar upper limits. Assuming a 9 keV spectrum, 1.3 times as much flux would be seen in the 2-20 keV band. Since the stars have masses of ~ 0.2 $M_0$, the computed 2-20 keV emissivity is about 1.5 x $10^{25}$ ergs $s^{-1}$ $pc^{-3}$. Given the large uncertainties in the calculation, this emissivity is comparable to the required emissivity of (3-6) x $10^{25}$ erg $s^{-1}$ $pc^{-3}$, and so halo stars cannot be eliminated as a major source of disk emission. It should be noted that the IPC is primarily responsive to temperatures of a few million degrees, not 100 million degrees. However, when Swank and White (1980) looked at late type stars with the HEAO 2 SSS instrument which is sensitive to both energy ranges, they found that the stars studied required two temperature fits at ~ 7 and ~ 50 million degrees with the hotter temperature about twice the luminosity of the lower. Although the stars studied were <u>not</u> halo stars, their results give some encouragement that

there may be some correlation between the energy band observable by the IPC and the emission energy band indicated by the spectrum for the disk emission).

Although the X-ray luminosity function for subdwarfs is not well known, we can estimate the required optical to X-ray luminosity ratio if the subdwarfs are to provide the bulk of the disk emission. Eggen (1979) indicates that optical luminosity function of halo stars is steeper than that for normal dwarfs. In Table 3 we estimate the required optical to X-ray luminosity for what we consider two bounding approximations to the mass function: that subdwarfs have the same mass function as normal dwarfs and that all subdwarfs are sdM5 stars. It appears possible that subdwarfs could provide the disk emission implied by the finite disk model. Observations of the X-ray luminosity of subdwarfs, particularly of their luminosities in the 100 million degree Kelvin range, should be able to confirm or reject this emission mechanism in the near future.

With their sensitivity of about $3 \times 10^{-14}$ ergs $cm^{-2}$ $s^{-1}$ in the 1 to 3 keV band the deep sky surveys (Giacconi et al. 1979) of the Einstein Observatory (HEAO-2) would detect $6 \times 10^{27}$ erg/s sources radiating a 9 keV thermal spectrum only out to a distance of ~ 25 parsecs. Therefore only about 0.013 halo stars per square degree would be detected if these stars had the average properties described above. In order to contribute a non-negligible portion of the observed sources, the X-ray luminosity of these objects in the 1-3 keV band of the Einstein Observatory deep survey would have to be an order of magnitude larger than the corresponding 9 keV component described above.

## VII. HOT GAS HALO

In 1956 Spitzer proposed that the Galaxy might have a halo of hot gas which is in hydrostatic equilibrium in the galactic gravitational field. Assuming that the gas was in pressure equilibrium, he estimated a halo

temperature of $10^6$ °K and a particle density of $10^{-3}$ cm$^{-3}$ as reasonable parameters for this halo. (At the time, the pressure, P/K ~ nT, was thought to be ~ $10^3$ K cm$^{-3}$ for the interstellar medium.) He pointed out that if the temperature were too high, the gas would escape from the Galaxy and if the temperature were too low, the "halo" would not extend far.

The best fit parameters of our X-ray emission disk imply, for a hot plasma of hydrogen and 10% helium, an electron density in the galactic plane of ~ 2 x $10^{-4}$ cm$^{-3}$. This is a pressure of P/k ~ 20,000 K cm$^{-3}$, a pressure within the range of 10,000-20,000 K cm$^{-3}$ now thought typical of the interstellar medium by some authors (e.g., Shapiro and Field 1976). The energy needed to resupply the halo against its radiation losses, ~ $10^{39}$ ergs s$^{-1}$, could easily be resupplied by one supernova every 25 years depositing only a tenth percent of its energy into the halo.

However, as Spitzer first pointed out, gas with a temperature beyond a few tenths of a keV is not bound by the Galaxy's gravitational field. At 9 keV, protons have a velocity of 1300 km/s (~ 1.3 kpc/Myr). The escape velocity for the Galaxy at a radius of 10 kpc and height of 5 kpc is ~ 300 km/s (Allen 1973). Gas with a temperature of 9 keV could be gravitationally bound only within about 1 kpc of the galactic center.

We can make a crude estimate of the timescale for gas to escape the Galaxy by dividing the scale height by the average particle velocity, t ~ h/v ~ a few million years. If the halo were a steady state phenomenon, it would be losing mechanical energy at the rate of $10^{43}$ erg s$^{-1}$. While supernovae might supply this energy, the mass loss rate (~ 20 $M_0$/yr) implies that, over the course of the Galaxy's lifetime, the Galaxy would have lost 3 x $10^{11}$ solar masses. This is greater than the current mass of the Galaxy. Thus such a hot gas halo must either be transitory or else it must be held by

something else in addition to the disk mass of the Galaxy.

The massive galactic halos proposed by Ostriker (1979) and others, could not provide support for the hot gas because only the mass interior to the observed X-ray disk would help to confine it.

A salient possible mechanism for confining such a halo of hot gas would be via a magnetic field. For a randomly oriented field to pressure balance the hot gas would require a field strength of ~ 10 microgauss. A partially aligned field could, of course, be somewhat lower. Field strengths as high as 6-10 microgauss have commonly been surmised from radio synchrotron measurements in the galactic plane (Webster et al. 1979). Large scale magnetic features have been reported by Simard-Normandin and Kronberg (1980). For a uniformly distributed magnetic field, the implied energy in the field is about twice the energy implied in the hot gas (~ 4 eV/cm$^3$ vs ~ 2 eV/cm$^3$).

If a hot (40 keV) intergalactic medium were to confine the galactic halo, that IGM would have to have a local density (e.g., within the local supercluster) comparable to the closure density of the universe.

While the model of a hot gas halo producing the observed "diffuse" galactic emission cannot be absolutely ruled out at this time, the problems of maintaining the halo or of producing a galaxy-wide burst are extremely severe.

## VIII. INVERSE COMPTON EMISSION

This model is, in a sense, the oldest of the proposed models for the galactic X-ray thick disk emission. In 1947 Follin first realized the inverse Compton mechanism to be an important energy drain on cosmic ray electrons, and in 1959 Savedoff discussed its possible importance in producing X-rays and $\gamma$-rays in the Crab nebulae. Warwick et al. (1980) and Protheroe, Wolfendale, and Wdowczyk (1980) have proposed the inverse Compton mechanism as the likely

source of the galactic hard X-ray background seen in the Ariel V and Uhuru data, respectively.

In this model, cosmic ray electrons produce the X-ray halo by inverse Compton emission off of the 2.7 $^{o}$K microwave background (and optical starlight and infrared emission). These same cosmic rays also produce radio synchrotron emission as they spiral in the galactic magnetic field and $\gamma$-rays by bremsstrahlung as they collide with matter.

We test whether the inverse Compton mechanism can provide the observed X-ray emission by two approaches. First, we calculate the expected inverse Compton emission by assuming that the interstellar electron spectrum deduced by Rockstroh and Webber (1978) interacts with the microwave background (following Cowsick and Kobetich 1972). Alternatively, we simply assume that there exists some power law electron spectrum which gives rise to a power law X-ray spectrum.

If the deduced interstellar electron spectrum is used, the calculated 2-10 keV inverse Compton emission is a factor of 11 (6) too low for a scale height of 3 kpc (7.3 kpc) and resembles a thermal spectrum in our detectors only if $kT \gtrsim 100$ keV.

As was discussed earlier, the averaged galactic spectrum is poorly fit by a power law model. It is unlikely that more than a third of the averaged galactic spectrum is due to a power law component and hence could be due to an inverse Compton mechanism.

Both of these methods indicate that the inverse Compton effect can provide neither the spectrum nor the intensity of the observed X-ray (thick disk) emission unless (a) the intensity and spectral distribution of distant GeV electrons is very different from the spectrum of local cosmic rays or (b) the dominant spatial feature of the galactic X-ray background seen in our

detectors is not strongly coupled to the dominant spectral feature seen.

Still, it is useful to consider the inverse Compton mechanism in more detail because it almost surely provides at least a few percent of the X-ray background and because some of the caveats listed in the preceeding paragraph may hold true.

From Ginzburg and Syrovatskii (1964), the intensity of inverse Compton emission goes as

$$6)\quad I_X(>E_X) \text{ photons cm}^{-2}\text{ s}^{-1}\text{ sr}^{-1} = 3.9 \times 10^{-3}\,(2.5 \times 10^3)^{m-1} \times f(m) \times \left(\frac{R}{7.5\text{ kpc}}\right) \times \left(\frac{\rho}{0.3\text{ eV/cm}^3}\right) \times \frac{1}{m-1} \times K_e\, E_X^{\frac{-m-1}{2}}$$

where $I_X(>E_X)$ is the flux for photon energies greater than $E_X$, m is the electron spectral index, f(m) is a function given in Ginzburg and Syrovatskii (1964) and approximated in Table 4, R is the scale height, $\rho$ is the density of the ambient field, $K_e$ is the number of cosmic ray electrons $\text{cm}^{-2}\text{ s}^{-1}\text{ sr}^{-1}\text{ GeV}^{(m-1)}$ and $E_X$ is the observed photon energy in eV.

Because the 2.7° K photon field is isotropic, the inverse Compton emission depends only on the cosmic ray electron "scale height". Because we expect optical and infrared emission to be confined more to the plane, we do not specifically calculate them here. However, the equations are stated in such a form that, once a space distribution for their emission is assumed, their contribution may be added in.

Radio synchrotron emission and $\gamma$-ray bremsstrahlung emission have smaller scale heights than the thick disk. However, they depend not only on the distribution of cosmic ray electrons, but also on the distribution of magnetic field (as $\sim B^2$) and matter (as $\sim n_0$), respectively. Thus, for example, the $\gamma$-ray emission is confined to the galactic plane by matter (see, for example, Fichtel et al. 1979). Some authors (e.g., Brindle et al. (1978)) and Webster (1978) have fit the radio data to a large scale height halo component as well as disk and extragalactic components. But, even if the bulk of the galactic radio emission does come from within 500 pc of the plane, it might be that only the magnetic field (but not the cosmic ray electrons) had this small a scale height. Thus any possible inconsistency between the radio scale height and the thick disk hard X-ray scale height could be resolved.

TABLE 4

| m | 1 | 2 | 3 | 4 |
|---|---|---|---|---|
| f(m) | 0.84 | 0.86 | 0.99 | 1.4 |

The spectrum of the averaged galactic hard X-ray emission is the more difficult data to resolve with the inverse Compton emission mechanism, since the spectrum of the cosmic ray electrons determines the X-ray spectrum. If we assume that the cosmic ray electrons and X-ray emission can both be fit by a power law spectrum, then for an electron spectral index of m, the X-ray photon spectral index, $\alpha$ , is (m+1)/2. where

7) $I_e(E) = K_e E^{-m} dE.$

For a black body ambient photon field of temperature T, the energy of the scattered photons, $E_x$, is related to the energy of the scattering cosmic rays, $\gamma m_o c^2$, as

8) $E_x \approx \frac{4}{3} (2.7\ kT)\ \gamma^2$

(Ginzburg and Syrovatskii 1964). Most of the observed galactic X-ray emission comes from the energy range 2 to 12 eV. If this X-ray emission arises from a $2.7^o$ K field, the implied cosmic ray elcctron energies are 700 MeV to 1.5 GeV. Table 5 summarizes the cosmic ray electron spectrum as observed at the earth over this energy range (see Rockstroh and Webber 1978; Weber et al. 1980).

TABLE 5

| ELECTRON ENERGY | m |
|---|---|
| < 1/2 GeV | 2.14 ± 0.06 |
| 1-10 GeV | 3.0 |
| > 10 GeV | 3.4 |

Using Equation 7 and our fit to the X-ray data, we can compare the cosmic ray electron density required to produce the observed X-ray flux with that

flux observed in the local interstellar medium. According to Rockstroh and Webber (1978), at 1 GeV, $I_e \approx 1.5$ to 3. $\times 10^{-3}$ electrons $cm^{-2}$ $sr^{-1}$ $s^{-1}$ $GeV^{-1}$, where the bulk of the scatter is due to different observations taken at different parts of the solar cycle. The higher number is probably more appropriate and we use it throughout this discussion. The observed cosmic ray electron density at the earth falls a factor of 20 short of producing the X-ray emission implied by a 7.3 kpc scale height and a factor of 40 short of that implied by a 3 kpc scale height.

At 1 GeV, cosmic ray electrons still suffer marginally from solar modulation; this can account for as much as factor of 2 or 3 in the discrepancy of the X-ray flux. Radio observers (e.g. Webber et al. 1980) have proposed that the sun may be in a local minimum of cosmic ray electrons, and that the ambient galactic cosmic ray electron densities might be a factor of ~ 8 higher than the local density. Of course, it is also possible that the radio synchrotron intensities are higher than expected because of higher magnetic fields. Similarly, the $\gamma$-ray intensities are higher than one would expect from the local cosmic ray and matter densities. The $\gamma$-ray data implies that either $n_0$ or the cosmic ray density or both be higher by a factor of ~ 4 throughout the Galaxy than they are locally (Fichtel et al. 1979). Thus, depending on what assumptions we make for the cosmic ray electron density, we might expect between about 3% and 30% of the X-ray disk emission to be due to the inverse Compton mechanism. These limits are comparable to those obtained from the averaged spectrum alone.

Protheroe et al. (1980) have stated that the inverse Compton mechanism is consistent with their analysis of the Uhuru data. Since we have said that our data are not consistent with it and also that their local emissivity is within a factor of two of ours, we should also point that their estimate of the

inverse Compton flux due to the microwave background scattered from 1 GeV electrons is in agreement with our calculations. For these energies, they predict a flux of $1.2 \times 10^{-10}$ ergs $cm^{-2}$ $s^{-1}$ $sr^{-1}$ from the inverse Compton mechanism. About 1/3 of this flux is from scattering off the infrared photons and about 2/3 is from the microwave photons. Thus they predict $8 \times 10^{-11}$ erg $cm^{-2}$ $s^{-1}$ $sr^{-1}$ while our best fit to the data is $2.0 \times 10^{-9}$ ergs $cm^{-2}$ $s^{-1}$ $sr^{-1}$. Thus our data are a factor of 25 higher than their predictions for inverse Compton scattering off the microwave background. They get consistency with all the X-ray flux being due entirely to radiative processes due to relativistic particles by adding in a highly model dependent synchrotron term, by having a large range in their acceptable fits (of up to over an order of magnitude) and by having a lower best fit flux.

Their synchrotron component is larger than or comparable to their inverse Compton component, in the 2-20 keV band. This synchrotron component has a much steeper slope than the inverse Compton component (see Figure 2 of Protheroe and Wolfendale 1980). Therefore the summed spectrum must have a concave shape in the 2-20 keV band. However, our observational results show that the spectrum has a convex shape. We feel that this rules out the model of Protheroe and Wolfendale as the origin of the dominant galactic component of the diffuse X-ray flux.

## IX. CONCLUSIONS

The dependence of the 2-60 keV X-ray flux on galactic latitude and longitude indicates that about 2-10% of the emission seen is galactic in origin. This diffuse emission is describable by the model of a finite radius disk with a scale height of greater than ~ 1500 pc and a radius comparable to that of the stellar galactic disk. The averaged diffuse galactic spectrum is described by a thin thermal bremsstrahlung spectrum of kT ~ 9 keV with no

absorption beyond that of the known diffuse gas in the Galaxy. For such a spectrum, the lack of observed iron line emission indicates iron is underabundant by a factor of $\gtrsim 6$ compared to solar abundances. If we assume that the feature which dominates the spatial appearance of the data also dominates the spectrum, then two models seem promising to explain the bulk of this X-ray emission. The simplest of these is that emission may be due to subdwarf halo stars with typical X-ray luminosities of (1.9-3.8) x $10^{28}$ ergs $s^{-1}$ $M_{\odot}^{-1}$ at temperatures ~ 100 million K. We note, however, that the typical x-ray luminosity of such stars is not well known.

Alternatively, the diffuse halo might originate in a very hot gas ($T \sim 10^8$ K, $n_e \sim 2 \times 10^{-4}$ $cm^{-3}$) which is either in the process of bursting or else is contained by within the Galaxy by some mechanism in addition to the gravitational field of the disk itself. A magnetic field might supply this containment, but such a field would be much stronger than is currently thought to be the case. The containment mechanism poses a <u>severe</u> problem for this model.

The inverse Compton model is least preferred because of spectral discrepancies and the anomolously high cosmic ray electron density required. This mechanism probably provides less than ~ 1/3 of the averaged galactic emission. However, it might dominate individual components (such as a thin disk) of the averaged spectrum.

Observations of the X-ray luminosity function of the subdwarfs by telescope X-ray experiments would be helpful in testing the first model. More sophisticated models of the Galaxy might help in determining whether the second model is in fact feasible. A determination of the spatial dependence of the galactic spectrum may be retrievable from the entirety of the HEAO-1 A-2 data base.

## ACKNOWLEDGMENTS

The authors thank Jean Swank for her valuable discussions and assistance.

TABLE 1

COMPARISONS OF MAPS OF THE SKY

| MAPS COMPARED | $\chi^2$ | DEGREES OF FREEDOM |
|---|---|---|
| HED1 sky 2 vs. HED1 sky 1 | 3335.10 | 3351 |
| HED3 sky 2 vs. HED3 sky 1 | 2859.22 | 2750 |
| MED sky 1 vs. MED sky 2 | 2805.52 | 2630 |
| MED sky 1 vs. HED1 sky 1 | 2548.88 | 2478 |
| HED3 sky 1 vs. HED1 sky 1 | 4133.15 | 4131 |
| MED sky 1 vs. HED3 sky 1 | 4494.40 | 4515 |

TABLE 2

MODEL FOR SCALE HEIGHT

| PARAMETER | 3 kpc | 7.3 kpc | 10 kpc | (3 kpc + 450 pc) |
|---|---|---|---|---|
| $R_d$(kpc) | 18 | 28 | 33 | 14 |
| Emissivity in plane | 5.8 | 3.2 | 3.3 | (4.6 + 8.5) |
| ($10^{25}$ ergs/(s-pc$^3$)) | | | | |
| ($10^{-31}$ ergs/(s-cm$^3$) | 19.7 | 10.9 | 11.2 | |
| (2-20 keV) | | | | |
| Flux to zenith (c/s) | 0.088 | 0.12 | 0.17 | (.069 + .020) |
| ($10^{-9}$ ergs/(s-cm$^2$ sr)) | 1.4 | 2.0 | 2.8 | (1.1 + 0.3) |
| (at 2-20 keV) | | | | |
| Galactic luminosity | | | | |
| ($10^{38}$erg/s) | 3.9 | 8.1 | 22 | 2.3 |

TABLE 3

SUBDWARF MODELS

| MODEL FOR MASS FUNCTION | OPTICAL LUMINOSITY $10^{25}$ ergs $s^{-1}$ $pc^{-3}$ | $L_{opt}/L_x$ REQUIRED |
|---|---|---|
| As normal dwarfs, all classes, F-M, included | 200,000 | $\sim 10^5$ |
| All subdwarfs are sdM5 | 40 | 10-20 |

## FIGURE CAPTIONS

Figure 1 - An Aitoff projection of the sky as seen with the HEAO 1 A2 HED1 xenon proportional counter. Data is taken from 2 to 60 keV for the large-minus-small field of view data from day 322 to 697 of 1976. Resolved sources have been eliminated down to better than $\sim 5 \times 10^{-11}$ erg $s^{-1}$ $cm^{-2}$. Each line per pixel represents 1.5% of the mean intensity starting at 10.5% below the mean. That is, 1-7 lines indicates an intensity below the mean, while 8 or more lines indicates an intensity above the mean. Pixels are $9^0 \times 9^0$. "Missing" pixels within the map represent regions where a complex of resolved sources prohibited any data collection. The median standard deviation is ~ 1.5% of the mean intensity (i.e. ~ 1 line per pixel). However, coverage varies considerably over the map both because the ecliptic poles are scanned more than the ecliptic plane and because resolved sources in some pixels severely limit data acquisition. Pixels with standard deviations greater than 3.75% are enclosed in dashed lines. The darker pixels near the galactic plane may be enhanced by unresolved point sources as well as the enhanced galactic emission towards the plane.

Figure 2 - The count rate for the HED1 detector from 2-60 keV for the large-minus-small field of view is plotted in Figure 2a as a function of galactic latitude for two regions of galactic longitude. ($-90^0 < \ell < +90^0$ and $90^0 < \ell < 270^0$). The count rates show a clear dependence on both galactic latitude and galactic longitude. For reference, an estimate of the magnitude of the maximum Compton-Getting effect predicted by the microwave data is included. This effect is ~ 0.5% of the mean X-ray intensity at the poles. In Figure 2b only the lower energy part of layer 1 of HED1 (that below ~ 6.7 keV) is

plotted. In Figure 2c only the higher energy part of layer 1 of HED1 (that part above the 6.7 keV iron ) is plotted. In Figure 2d only the layer 2 count rates of HED1 are plotted. This layer has a response primarily from 6 to 60 keV.

Figure 3 - In panel (e) the X-ray intensity is plotted versus absolute galactic longitude for various ranges of latitude. That is, the four "quadrants" of the Galaxy have been averaged together to aid in seeing the overall effects of the galactic emission. Notice that the data vary with galactic longitude even for high galactic latitudes (e.g. at $24^{0} < |b| < 45^{0}$). For comparison predictions of various models shown are in the other panels with the $\chi^2$ and degrees of freedom (dof) obtained when fitting the model to the data.

Figure 4 - The X-ray intensity is plotted as a function of galactic latitude for several ranges of galactic longitude. Above $|b| \sim 30^{0}$, there is little variation of intensity with longitude, but at lower latitudes the variation is strong.

Figure 5 - This figure shows the $\chi^2$ minimum + 5.99 (~ 95% confidence) contour for the scale height and disk radius parameters for the finite radius disk model for the HED1 2-60 keV, large-minus-small fov data. The distance to galactic center is assumed to be 10 kpc for this figure. $\chi^2$ minimum is 3241 for 3026 dof (only when smaller features are included in the fit does $\chi^2$ drop to about the number of degrees of freedom). The $\chi^2$ +5.99 contour presented here is actually smaller than the true 95% confidence contour for this model because other features have some affect on the fit of this model to the

data. These other smaller features do not change the general nature of the contours; rather they expand the contours somewhat.

Figure 6 - The HED1 2-60 keV count rate is plotted as a function of galactic longitude for two latitude 6 bins. For reference, the best fit model prediction at b = $15^{0}$ is included. Within ~ $30^{0}$ of the plane, we might expect most of the variation in count rate to be due to galactic effects. Note that the variations in this figure do not go smoothly with longitude. Thus no simple model will predict them well.

Figure 7 - This figure shows the 95% upper limits to a power law contribution to the galactic spectrum for various power law indices. Both the temperature of the isotropic background (40 keV) and of the dominant galactic component (9 keV) were fixed in preparing this figure. If these temperatures are allowed to vary drastically, the power law components can be made larger. However, if the temperatures are only allowed to vary within a few sigma of their best fit values, then this upper limit curve does not change significantly.

## REFERENCES

Allen, C.W. 1973, "Astrophysical Quantities", The Athlone Press, New York.

Bleach, R.D., Boldt, E.A., Holt, S.S., Schwartz, D.A., and Serlemitsos, P.J. 1972, Astrophys. J. 174, L101.

Blaauw, A., "The Concept of Stellar Populations", p. 435, ed. A. Blaauw and M. Schmidt "Galactic Structure" (1965, U. of Chicago Press, Chicago).

Bessell, M.S. and Wickramasinghe, O.T. 1979, Ap. J. 227, 232.

Brindle, C., French, O.K. and Osborne, J.L. 1978, MNRAS 184, 283.

Cane, H.V. 1978, Astr. J. Phys. 31, 561.

Cane, H.V. 1979, MNRAS 189, 465.

Cesarsky, D.J., Paul, J.A., and Shukla, P.J. 1978, Ap. and Sp. Sci 59, 73.

Chevalier, R.A. and Oegerle, W.R. 1979, Ap. J. 227, 398.

Condon, J.J. 1974, Ap. J. 188, 279.

Cowsik, R. and Kobetich, E.J. 1972, Ap. J. 177, 585.

Cunningham, G., LloydEvans, J., Pollock, A.M.T., Reid, R.J.O. and Watson, A.A. 1980, Ap. J. 236, L71.

Eggen, O.J. 1979, Ap. J. 229, 158.

Eggen, O.J. 1979, Ap. J. 230, 786.

Felten, J.E. and Morrison, P. 1966, Ap. J. 146, 686.

Fichtel, C.E., Simpson, G.A. and Thompson, D.J. 1978, Ap. J. 222, 833.

Follin, J.W. 1947, Phys. Rev. 72, 743 (Abs.).

Giacconi, R. et al. 1979, Ap. J. 234, L1.

Gilman, D., Metzger, A.E., Parker, R.H. and Trombka, J.I. 1979, Ap. J. 229, 753.

Ginzburg, V.L. and Syrovatskii, S.I. 1964, The Origin of Cosmic rays, Pergamon Press, New York.

Greenstein, J.L. 1965, "Subluminous Stars", p. 361, ed. A. Blaauw and M. Schmidt, Galactic Structure (1965, U. of Chicago Press, Chicago).

Higdon, J.C. 1979, Ap. J. 232, 113.

Johnson, H.M. 1981, Ap. J. 243, 234.

Lampton, M., Margon, B. and Bowyer, S. 1976, Ap. J. 208, 177.

Lugger, P.M. 1978, Ap. J. 221, 745.

Marshall, F.E., Boldt, E.A., Holt, S.S., Miller, R., Mushotzky, R.F., Rose, L.A., Rothschild, R.E., and Serlemitsos, P.J. 1980, Ap. J. 235, 4.

Oort, J.H., "Stellar Dynamics", p. 455 in ed. A. Blaauw and M. Schmidt, "Galactic Structure" (1965: U. of Chicago Press, Chicago).

Prince, Thomas A. 1979, Ap. J. 227, 676.

Protheroe, R.J. and Wolfendale, A.W. 1980, Astronomy and Astrophysics 92, 175.

Protheroe, R.J., Wolfendale, A.W., and Wdowczyk, J. 1980, MNRAS 192, 445.

Rockstroh, J.M. and Webber, W.R. 1978, Ap. J. 224, 677.

Rothenflug, R., Rocchia, R. and Casse, M. 1979, Ap. J. 229, 669.

Rothschild; R.E. et al. 1979, Space Sci. Instr. 4, 269.

Savedoff, M.P. 1959, Nuovo Cimento 13, 12.

Schlickeiser, R. and Thielheim, K.O. 1977, Ap. and Space Sci. 47, 415.

Schwartz, D.A., Murray, S.S., Gursky, H. 1976, Astrophys. J. 204, 315.

Schwartz, D.A. 1979, "COSPAR X-Ray Astronomy, ed. W.A. Baity and L.E. Peterson, Pergamon Press, Oxford and New York) 453.

Sharp, N.A. 1979, Astron. and Astrophys. 74, 308.

Simard-Normandin, M. and Konberg, P.P. 1980, Ap. J. 242, 74.

Spitzer, L. 1956, Ap. J. 124, 20.

Stecker, F.W. 1979, ed. W.P. Burton, "The Large Scale Characteristics of the Galaxy", p. 475.

Stecker, F.W. and Jones, F.E. 1977, Ap. J. 217, 843.

Swank, J.H. and White, N.E. 1980, NASA Technical Memo 80655.

Stromgren, B., "Stellar Models for Main-Sequence Stars and Subdwarfs", p. 269, ed. L.H. Allen and D.B. McLaughlin, "Stellar Structure" (1965, U. of Chicago Press, Chicago).

Warwick, R.S., Pye, J.P. and Fabian, A.C. 1980, MNRAS 190, 243.

Weaton, W.A. 1976, Ph.D. thesis, Univ. of Calif. San Diego, UCSD SP76-01.

Webber, W.R., Simpson, G.A., and Cane, H.V. 1980, Ap. J. 236, 448.

Webster, Adrian 1978, MNRAS 185, 507.

Worrall, D.M., Marshall, F.E. and Boldt, E.A. 1979, Nature 281, 127.

Worrall, D.M., Marshall, F.E., Boldt, E.A., and Swank, J.H. 1982, Ap. J., in press.

GALACTIC LATITUDE




GALACTIC LONGITUDE

HEAO I A-2 (6-3)x3 FOV, 2-60 keV SOURCEFREE

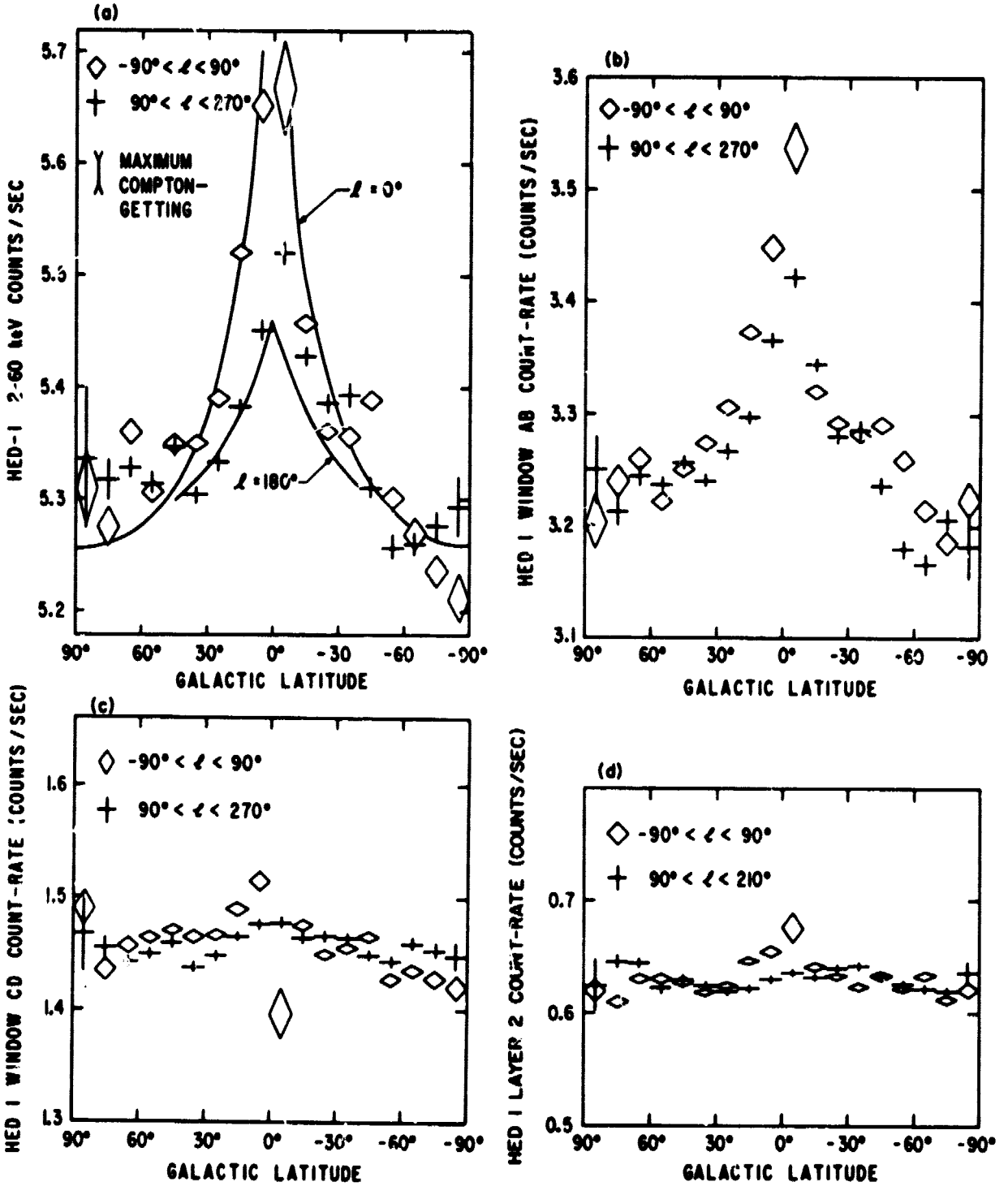

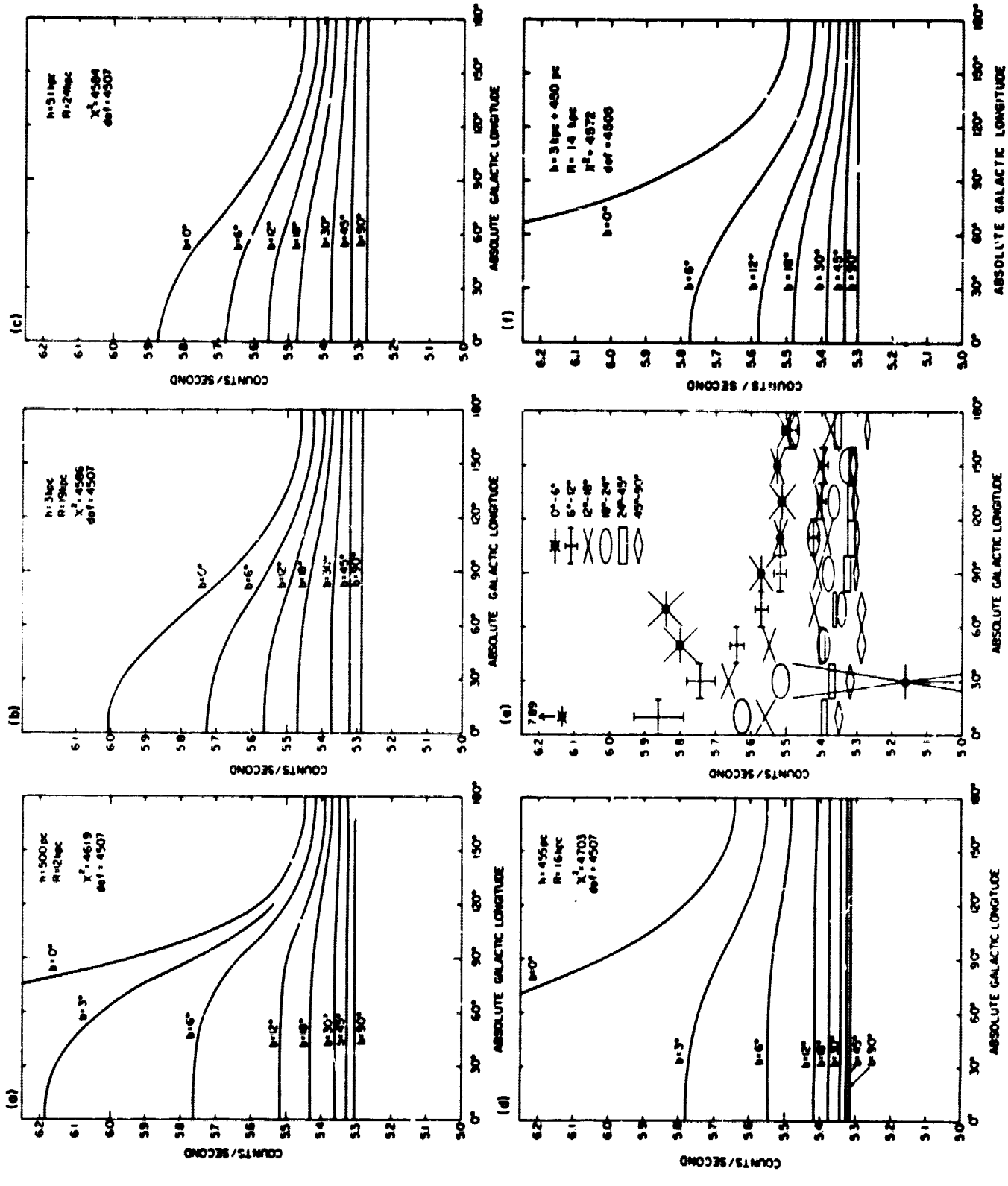

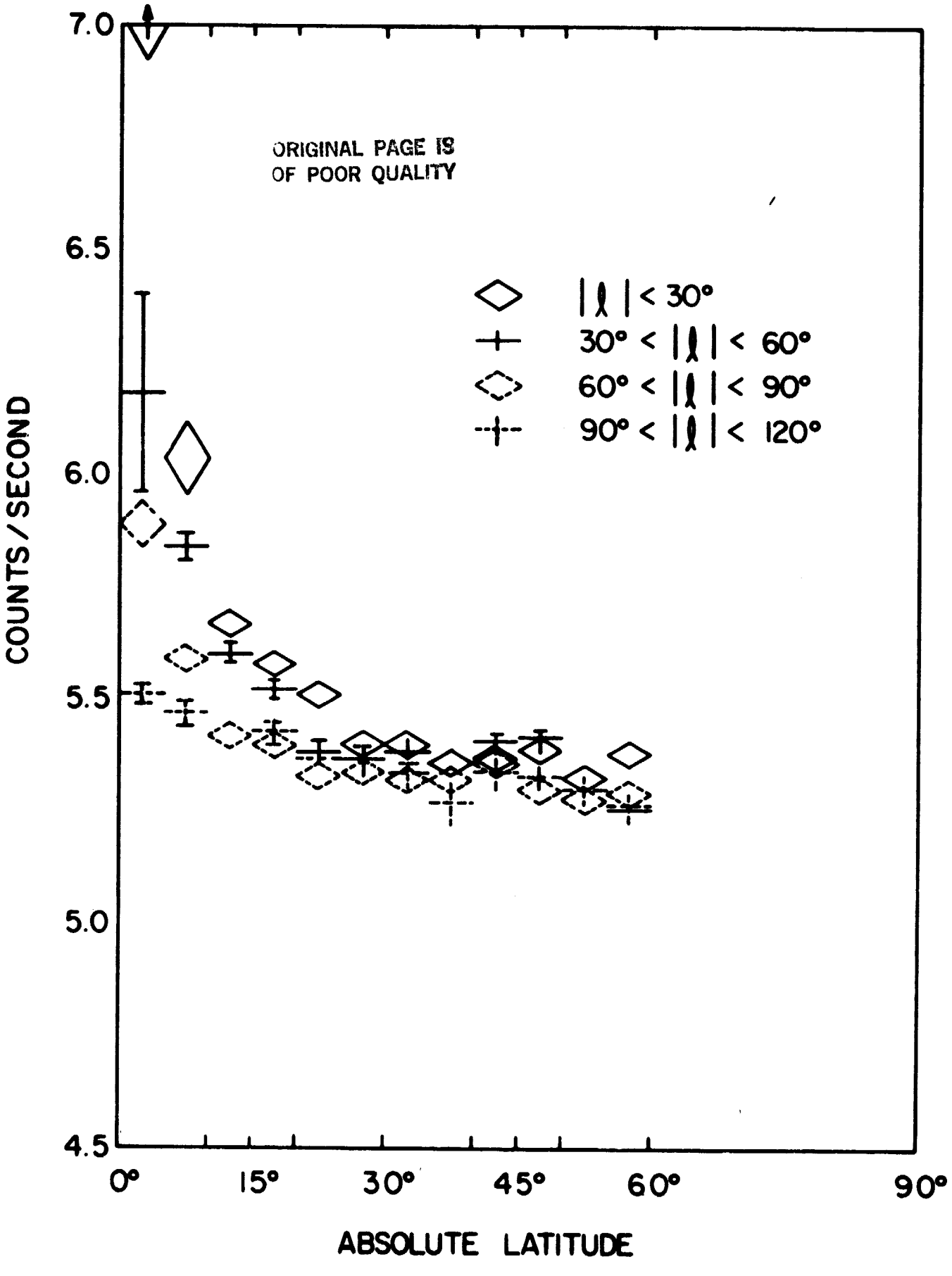
ORIGINAL PAGE IS
OF POOR QUALITY
|λ| < 30°
30° < |λ| < 60°
60° < |λ| < 90°
90° < |λ| < 120°
7.0
6.5
6.0
5.5
5.0
4.5
COUNTS/SECOND
0°
15°
30°
45°
60°
90°
ABSOLUTE LATITUDE

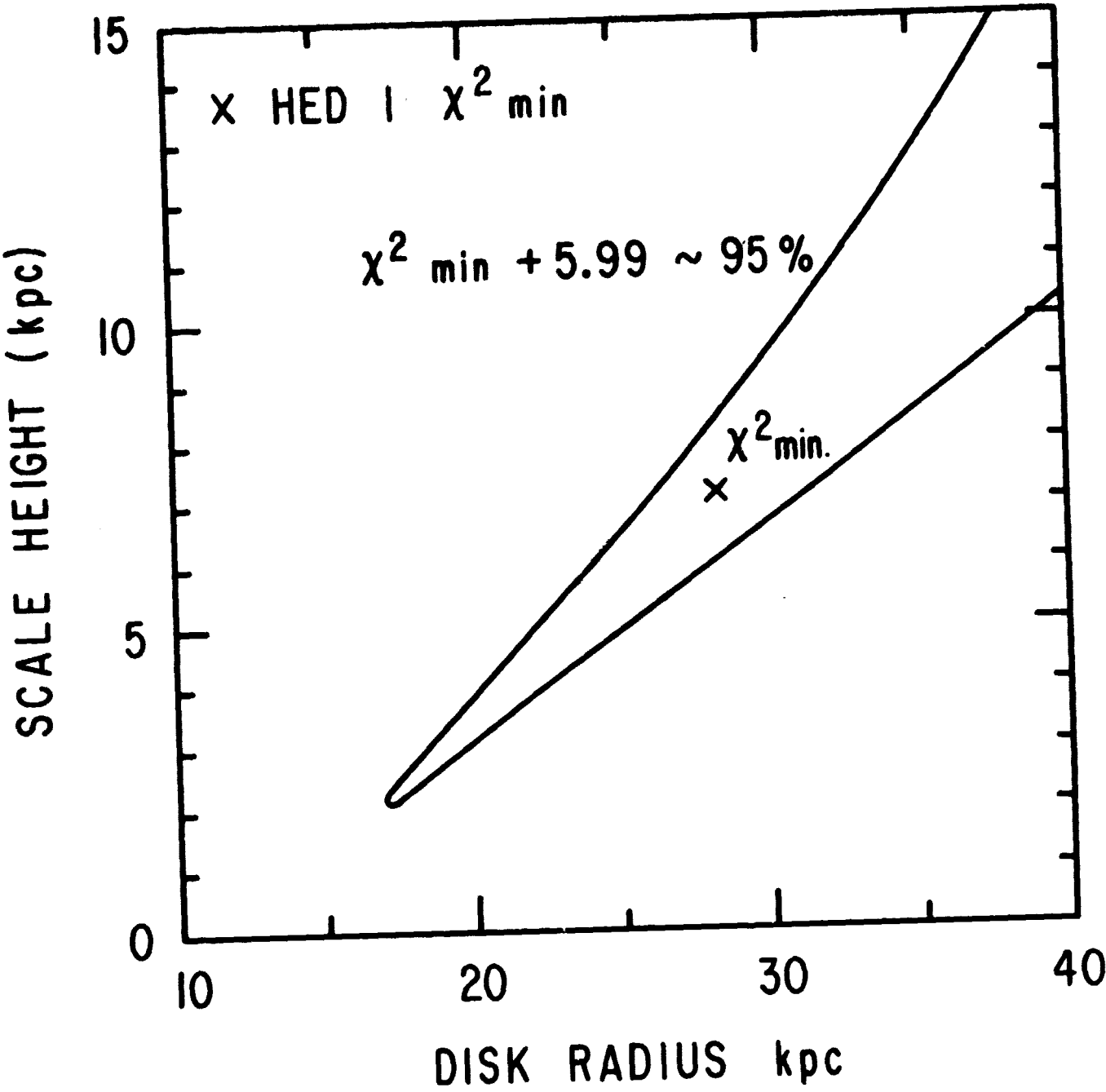

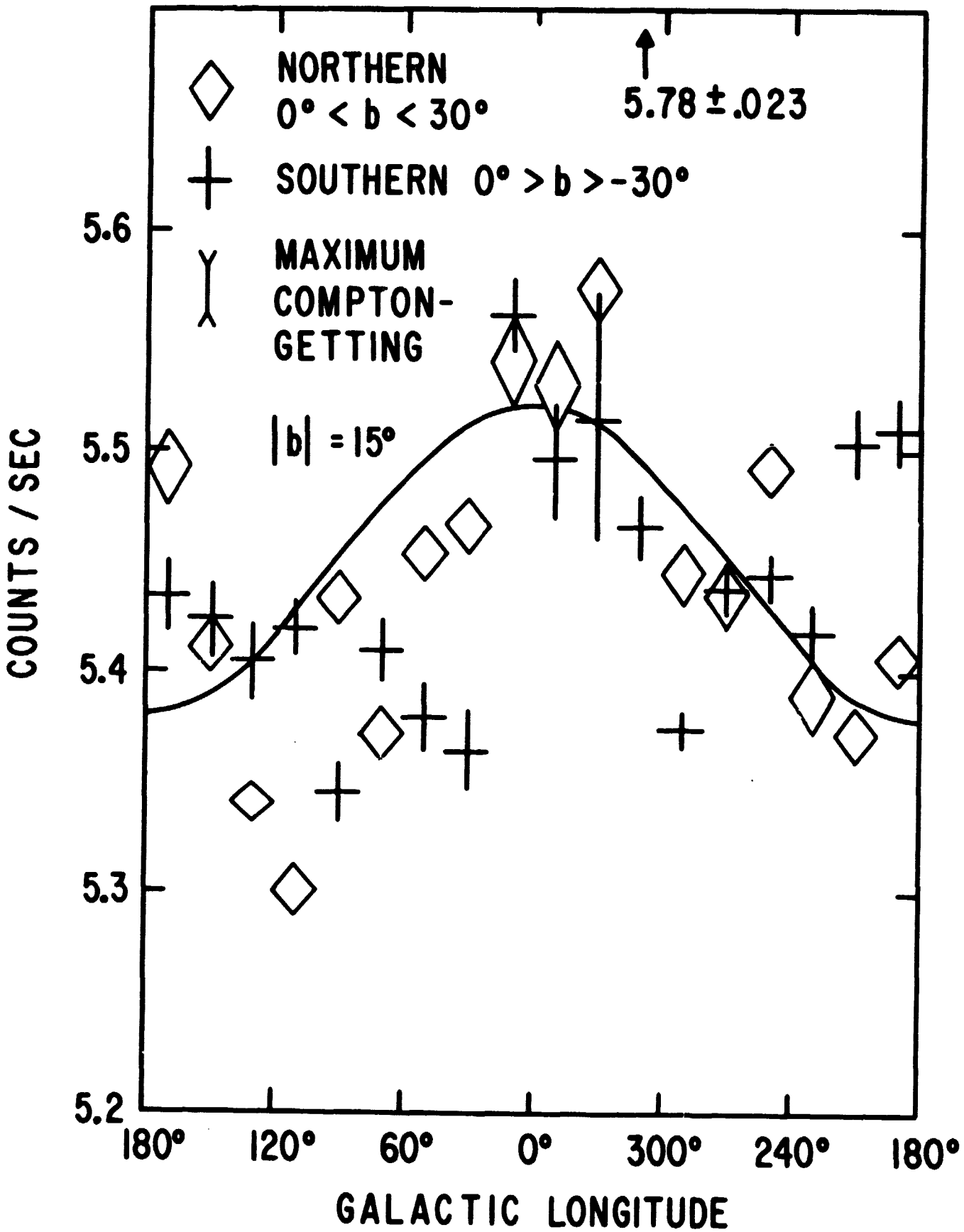

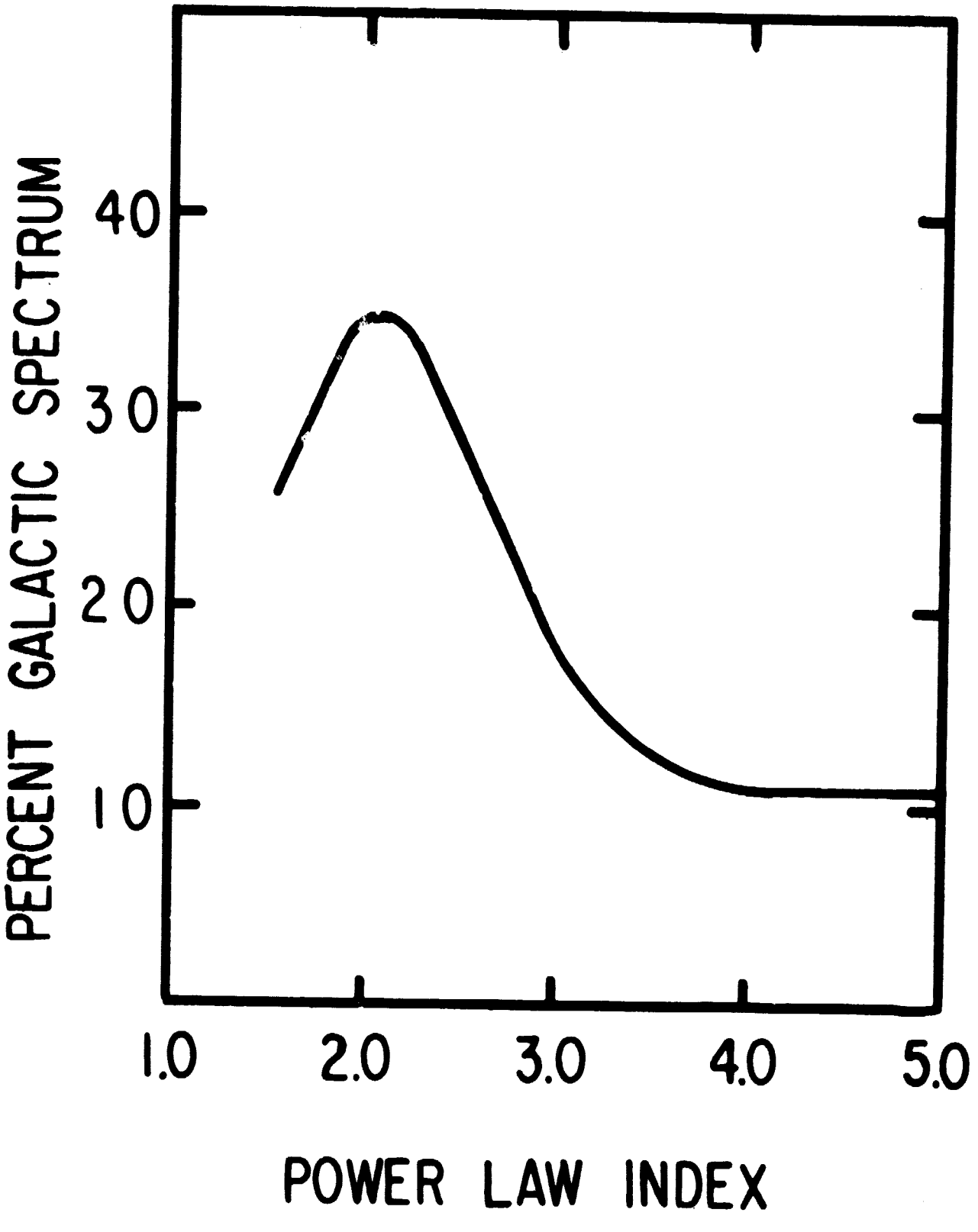

ADDRESS OF AUTHORS

E.A. BOLDT, DeANN IWAN, F.E. MARSHALL, R.F. MUSHOTZKY, R.A. SHAFER, Code 661, Laboratory for High Energy Astrophysics, NASA/Goddard space Flight Center, Greenbelt, MD 20771

and

A. STOTTLEMYER, Computer Science Corporation, Code 660, NASA/Goddard Space Flight Center, Greenbelt, MD 20771